***Annual Report: Role of confinement in coseismic pulverization of sediments: Testing the rock record of rupture directivity on the San Jacinto Fault (SCEC Award# 20027)***

**Principal Investigators**:
W. Ashley Griffith, School of Earth Sciences, Ohio State University
Thomas Rockwell, Department of Geological Sciences, San Diego State University

## 1. Key Points

- Motivated by field observations of incipiently pulverized (i.e., distributed fractures in grains, no to little shear strain) grains in the Bautista Formation adjacent to the San Jacinto fault at Rockhouse Canyon, we designed a suite of experiments designed to initiate the stress and strain-rate conditions necessary to produce the observed microstructures
- Experimental design involves dynamic loading of sediments in a confining cell using a split Hopkinson pressure bar
- Comparison of constitutive response of Ottowa Sand (well sorted, well rounded, primarily silica) and Bautista sediments (poorly sorted, sub angular, heterogeneous) yields smaller strains, larger stresses, and incipient cataclastic deformation band development in Ottowa sand, where primary brittle deformation mechanism is Hertzian fracture. In contrast, Bautista sediments experience large axial strains, smaller peak stresses, and distributed fractures in quartz grains due to lower contact stresses between poorly sorted sediments and phyllosilicates.

## 2. Summary

At Rockhouse Canyon, the San Jacinto fault juxtaposes Cretaceous tonalite against weakly to unconsolidated sediments of the Pleistocene Bautista Formation. Recent observations at Rockhouse Canyon have suggested that during earthquakes on the San Jacinto fault, Bautista Formation sediments transition from granular flow to grain crushing under a confining pressure between 1.4 and 2.4 MPa. Understanding this process informs us how to interpret the rock record of past earthquakes and provides constraints on the coseismic constitutive response of sediments. We test the hypothesis of a dynamic coseismic source of brittle damage at Rockhouse Canyoun using a modified Split-Hopkinson Pressure Bar (SHPB) apparatus, where sediments are packed into a cylindrical confining cell and plugged on both ends. A circumferentially mounted strain gauge monitors the dynamic confining pressure throughout an experiment, and traditional SHPB methods are used to calculate the axial stress, strain, and strain-rate data. Post-deformation experimental samples are preserved in epoxy resin for thin section preparation. Through this process, we seek to: (1) determine, experimentally, the stress states and strain-rates necessary to pulverize weakly to unconsolidated sediments, (2) compare experimental results to naturally deformed field samples in order to investigate past stress states and strain rates experienced along the San Jacinto fault, and (3) test the rock record along the San Jacinto fault for the potential of a preferred rupture directivity.

## 3. Introduction

Fault damage zones consisting of a particular brittle deformation style referred to as “pulverization” extend 10s to 100s of meters from their respective fault cores and represent off-fault inelastic deformation linked to dynamic earthquake rupture events (Doan and Gary, 2009). At the microscale, pulverized fault zone rocks (PFZR) are characterized by grain size reduction due to densely populated and pervasive microfractures, a virtual lack of shear strain leaving original fabrics recognizable, and a decay in fracture density with increasing distance from the fault core (Dor et al., 2006ab; Rempe et al., 2013; Rockwell et al., 2009; Wilson et al., 2005). On a larger scale, PFZR are most common at shallow crustal depths and exhibit asymmetric damage patterns across fault planes (Dor et al., 2006ab). The pulverization process has been tied to high strain-rates by experimental, numerical, and natural studies (e.g., Doan and Gary, 2009; Griffith et al., 2018; Johri et al., 2014; Xu and Ben-Zion, 2017; Whearty et al., 2017). Numerical modelling of dynamic rupture events, represented as a propagating Mode II fracture, produces a near-tip stress field characterized by an asymmetrical pattern of compressive and tensile mean

normal stress on either side of the rupture tip and peak strain rates approaching $10^4$ $s^{-1}$ within millimeters of the rupture tip (Reches and Dewers, 2005; Xu and Ben- Zion, 2017; Griffith et al., 2018). The high strain-rate requirement and asymmetric damage pattern suggests PFZR are likely fingerprints of past near-field earthquake rupture deformation and record information related to past stress-states, strain-rates, and rupture directivity (Rowe and Griffith, 2015).

At Rockhouse Canyon near Anza, California, the Clark strand of the San Jacinto Fault Zone juxtaposes Cretaceous tonalite of the northeastern side against poorly to unconsolidated sediments of the Pleistocene Bautista Formation on the southwestern side (Sharp, 1967). Recent work by Whearty et al. (2017) describes damage zone observations made at two fault transects of unique elevations and suggests the present pulverization is dependent upon burial depth (i.e., confining pressure), lithology, and distance from the fault core. Tonalite at the upper and lower transects have been exhumed from a depth of ~660 and 710m, respectively, and both exhibit characteristic pulverization fabric. Bautista sediments from the upper transect, where the exhumation depth is ~70m, show a microfracture density similar to off-fault background levels. However, at the lower transect where the exhumation depth reaches ~120m, Bautista sediments are interpreted to have reached the onset of pulverization with evidence in the form of densely populated, well-aligned microfractures of an average orientation orthogonal to fault strike and that decay in density from the fault core (Whearty et al., 2017). This depth dependence on pulverization prompted Whearty et al. (2017) to propose a minimal confining pressure exists between 1.4 and 2.4 MPa at which a transition occurs in Bautista sediments from granular flow to grain crushing, based on the maximum burial depths of ~70 and 120m and a sediment density of 2.0 g/cm$^3$. Furthermore, tonalite microfractures bear a striking resemblance to those produced experimentally through dynamic isotropic tension experiments (Griffith et al., 2018). Therefore, it seems likely that this deformation is the result of dynamic rupture based on the asymmetric distribution of damage (i.e., tensile and compressive side), confining pressure dependence, and microfracture density decay with increasing distance from the fault core (Whearty et al., 2017).

The observations at Rockhouse Canyon motivate our objectives by prompting such questions as: (i) what is the critical confining pressure at which brittle deformation initiates in Bautista sediments?; (ii) are the damage patterns suggestive of a potentially preferred earthquake rupture directivity?; and, (iii) more generally, what is the influence on confinement and strain-rate on the stress-strain response of sediments? Our experimental design, combined with the damage zone observations surrounding the Clark strand, offers a unique opportunity to extend the literature on the dynamic loading response of sediments, specifically in relation to the role of dynamic confining pressure and pulverization state. The potential for a preferred rupture directivity is of significant interest as well for its implications on seismic hazards such as strong ground motions (Abrahamson, 2000; Chen et al., 2018).

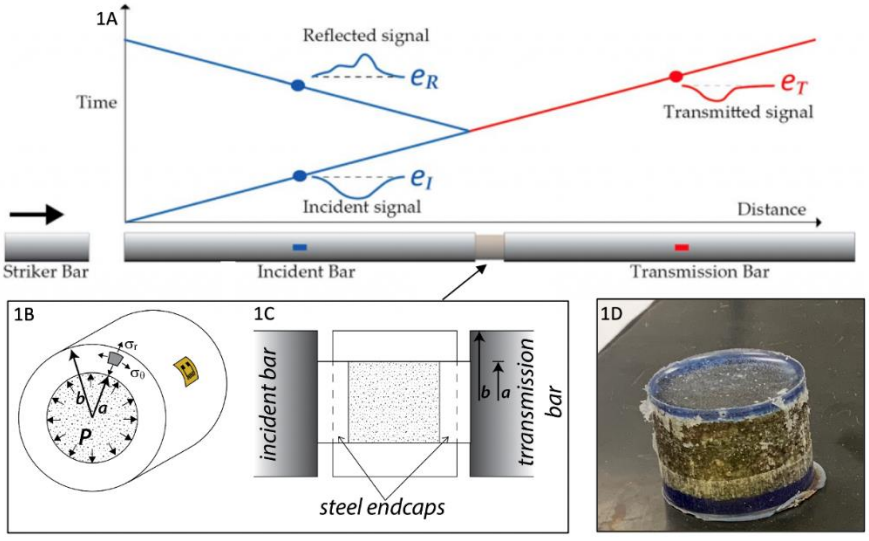


**Figure 1.** (A) Traditional Split-Hopkinson Pressure Bar assemblage and wave behavior. Dynamic force balance across the specimen is represented by $e_T e_I e_R$) .B) Circumferentially mounted strain gauge on the outer confining cell wall records circumferential strain ($e_\theta$) data to calculate the dynamic confining pressure ($P$) throughout an experiment. (C) Schematic drawing of cross-sectional view of SHPB mounted confining cell configuration. (D) Epoxy impregnated experimental sample ready for thin section preparation.

## 4. Methods

The SHPB is a commonly used tool for probing the constitutive behavior of materials under uniaxial compressive strain rates of $10^1$ to $10^3$ $s^{-1}$ (Doan and Gary, 2009; Xia and Yao, 2015; Griffith et al., 2018). Traditional SHPB experiments involve a cylindrical specimen, and three bars: a striker bar, incident bar and transmission bar. The specimen is placed between the incident and transmission bars. The striker bar is then fired by a projectile system, collides with the incident bar, and generates a compressive stress wave (incident pulse) that travels through the incident bar to the specimen (Figure 1A). The impedance contrast between the specimen and incident bar results in a portion of the compressive wave being reflected as a tension wave back into the incident bar (reflect pulse), and the remaining portion of the compressive wave travels through the sample to the transmission bar (transmitted pulse). Strain gauges on the incident and transmission bars record these transmitted and reflected energy data and, assuming 1D wave propagation and dynamic force balance across the two ends of the sample (i.e., incident and transmission ends), are used to calculate the axial stress, strain, and strain-rate throughout an experiment (Kolsky, 1949; Chen and Song, 2010; Xia and Yao, 2015).

In order to study the response of unconsolidated sediments to dynamic loading, the unconfined cylindrical specimen is replaced with a confinement cell following a modified version of the methods described by Bragov (2008) and Huang et al. (2014). The design consists of a hollow cylindrical jacket sealed on both ends by plugs of the same material and filled with sediment grains (Figure 1B,C). The transmitted portion of the uniaxial compressive stress wave now travels through the sediment column, and the resulting radial expansion will be limited by the inner wall of the confinement cell. Based on this design, the axial stress, strain, and strain-rate data are still determined as in a traditional experiment. An additional linear strain-gauge mounted to the external wall of the confining cell records the circumferential strain, $e_\theta$. The dynamic confining pressure is then solved for by the solution for a hollow linear elastic cylinder subjected to a uniform internal pressure (Lame, 1852; Timoshenko and Goodier, 1970), in which the radial and circumferential stresses within the cylinder are functions of the internal pressure, $p$, and the inner and outer radii of the cylinder, $a$ and $b$, respectively. Assuming plane stress conditions within the confining cell wall, the dynamic internal pressure normal to the sediment column is defined as $p = \frac{e_\theta E\,(b^2-a^2)}{a^2(1+\frac{b^2}{r^2})}$, where $E$ represents the Young's modulus of the confining cell and $r$ is the average of the inner and outer radii.

Our work consists of two sets of SHPB experiments. The first involves the confining cell configuration and 20-30 mesh Ottawa Sand in order to examine the dynamic loading response of a well-sorted, silica sand. The second set focuses on undeformed field samples of weakly to unconsolidated Bautista sediments. Damage in these specimens will ultimately be compared to field observations by Whearty et al. (2017) as well as new observations. Prior to all experiments, specimens in the confining cell are pre-compacted between 1.4 and 2.4 MPa by a uniaxial hydraulic press in order to accurately reflect the burial conditions described by Whearty et al. (2017) and to improve force balance during experiments. We have confirmed using thin sections that this pre-compaction does not result in grain scale fracture. The dynamic confining pressure among experiments is varied by controlling the Young's modulus of the cell material (i.e., steel or aluminum) and the applied axial load. Post-deformation specimens are preserved in epoxy resin within the confining cell in order to preserve the in-situ experimental deformation products for thin section preparation (Figure 1D).

## 5. Completed Work

During the reporting period, we have successfully implemented the new experimental design and completed initial set of Ottawa Sand and Bautista Formation confining cell experiments. We preserved post-mortem specimens in epoxy-resin, which were then cut in axis-parallel and axis-perpendicular sections for petrographic thin sections. Experimental data collected from these initial tests show fundamental differences in the dynamic response of Ottawa Sand and Bautista sediments to impulsive triaxial stress changes. For a given impact velocity of the striker bar into the incident bar, the axial and confining stress produced within Bautista sediments is much smaller than that of Ottawa Sand (Figure 2B). Simultaneously, despite similar initial conditions (e.g., average porosity of 34% in Bautista samples; 36% in Ottawa Sand), porosity reduction experienced by Bautista sediments is much greater than Ottawa Sand (Figure 2A). In general, for identical confining cylinder conditions, the ratio of axial stress to confining pressure is constant for both sediments, but at higher pressures above axial stress of ~35

MPa and dynamic confining pressure of ~15MPa the relationship becomes non-linear. Microstructural observations note that this deviation from linearity coincides with significant grain breakage and deformation band formation in Ottowas Sand. Granular materials accumulate strain under uniaxial compression by three mechanisms: (1) reorganization by frictional sliding of grains, (2) elastic compression of individual grains, and (3) grain size reduction by breakage and crushing (Whitman, 1970). Poorly sorted sands such as the Bautista Formation sediments are less prone to grain crushing than poorly graded sands (e.g., 20-30 Ottawa Sand) because the broader range of grain sizes leads to an increased number of grain contacts and, thus smaller stresses are produced at each contact (Kjaernsli & Sande, 1963; Whitman, 1970). The relatively high porosity reduction in Bautista sediments may be a result of low contact stresses favoring strain accumulation by grain reorganization rather than grain crushing or breakage. The larger normal stresses produced in Ottawa Sand experiments are also a likely reflection of this relationship between contact stresses and sediment grading.

**Figure 2.** (A) Relationship between experimental porosity reduction (%) and peak axial stress (MPa). Note: There is no significant difference in initial porosity between Ottawa and Bautista samples. (B) Peak dynamic confining pressure (MPa) in relation to peak axial stress (MPa). Green arrows mark experiments of equivalent impact velocity.

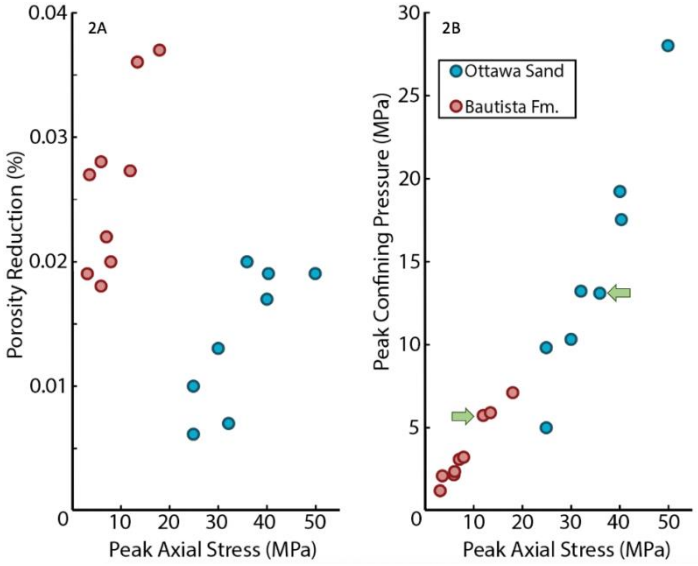


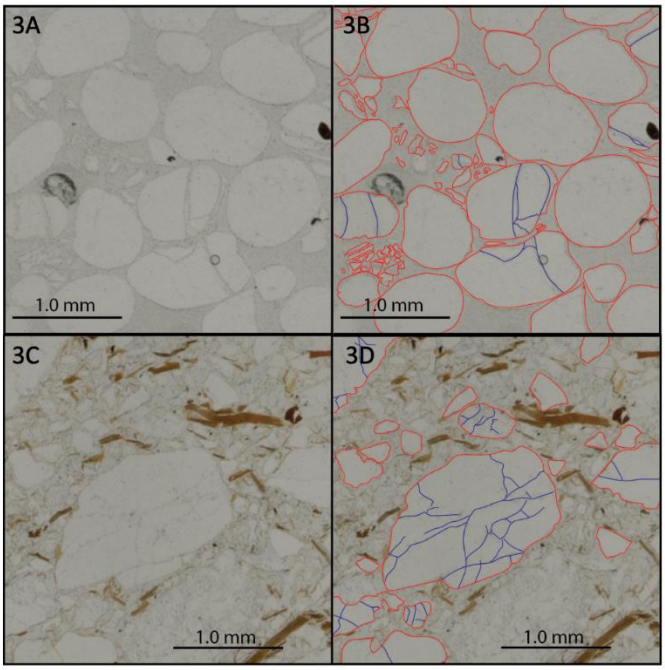


**Figure 3.** (A,B) Preliminary mapping of microfractures (blue) in quartz grains (red) of Ottawa Sand sample OS_12. Hertzian fractures dominate and a crushed grain exists in the bottom left of the image. (C,D) Preliminary mapping of microfractures (blue) in quartz grains (red) of Bautista sample BS_05. Note the concentration of phyllosilicates. Damage appears fundamentally different than Hertzian fractures, with limited crack nucleation from grain contacts. In both materials, fracture interpretations are mapped over PPL images but were constructed using both XPL and PPL.

The fingerprint of inelastic deformation in the well sorted, relatively uniform Ottawa Sand is predominantly in the form of Hertzian fractures propagating from grain contacts (Figure 3AB). These fractures appear to form in clusters (i.e., potentially "locked" zones of the sample) surrounded by patches of relatively undeformed grains.

Sample *OS_12* shows two sparce deformation bands of Hertzian fracture clusters normal to the axial direction. Bautista sediments collected from Rockhouse Canyon have a much more variable composition than Ottawa Sand, including a noticeably significant concentration of phyllosilicate minerals. Initial observations from thin sections further suggest a fundamental difference in the inelastic deformation of Bautista sediments, where microfractures preferentially form in relatively large quartz grains and lithic fragments but do not appear to nucleate from contacts between grains and qualitatively appear to vary from isotropic to weakly aligned to the axial direction (Figure 3CD). In both materials, there appear to be an increase in overall damage intensity (i.e., microfracture density) with increasing axial load, accompanied in the Bautista sediments by an increased alignment of phyllosilicate minerals. Quantitative analysis of microfracture mapping will reveal the true nature of the relationships between stress-state and strain-rate to overall damage state.

## 6. Upcoming Work

The qualitative observations made from thin sections of early experimental samples require quantitative analysis for validation. Microfracture analysis will be conducted using FracPaQ with the goal of mapping microfractures in density and orientation. Calculating the microfracture density of each sample and comparison to the hand-packed and press-packed standards will work to help pinpoint the minimal dynamic confining pressure required to reach the onset of grain crushing and to reveal information of past stress and strain conditions along the San Jacinto fault at Rockhouse Canyon. Understanding the orientation of experimental microfractures will have implications for comparison to the field samples (Whearty et al. , 2017), in which microfractures of large quartz grains are preferentially oriented orthogonal to fault strike. Further SHPB experiments will be performed using the confining cell configuration on Ottawa Sand and Bautista sediments in order to obtain a dataset more focused on teasing out the onset of grain crushing and using an isotropic tension configuration on cross-fault tonalite in order to test the local hypothesis of preferred rupture directivity.

We will conduct field work in Autumn 2021 to collect samples and to investigate sparse deformation bands at the Rockhouse Canyon field site. Reconnaissance field work in February 2021 revealed a few widely spaced deformation bands that were not described by Whearty et al. (2017). Given the lack of deformation band formation in experiments, we will explore the hypotheses that deformation band formation was related to long term secular deformation and/or larger total strains that we can simulate during SHPB experiments.

### Schedule for Completion

- Spring 2021
    i. Continued confining cell experimentation
    ii. Isotropic tension experimentation
    iii. Thin section analysis and post-experiment data collection
- Summer 2021
    i. Continued thin section analysis and post-experiment data collection
    ii. Write manuscript for related journal article
- Fall 2021
    i. Field work
    ii. Submit manuscript to Journal of Geophysical Research or Bulletin of the Seismological Society of America

## 7. References


Abrahamson, N. A. (2000, November). Effects of rupture directivity on probabilistic seismic hazard analysis. In *Proceedings of the 6th international conference on seismic zonation* (Vol. 1, pp. 151-156). CA: Palm Springs.

Bragov, A. M., Lomunov, A. K., Sergeichev, I. V., Tsembelis, K., & Proud, W. G. (2008). Determination of physicomechanical properties of soft soils from medium to high strain rates. *International Journal of Impact Engineering*, *35*(9), 967-976.

Chen, K., Feng, W., Liu, Z., & Song, Y. T. (2018). 2017 Mw 8.1 tehuantepec earthquake: deep slip and rupture directivity enhance ground shaking but weaken the tsunami. *Seismological Research Letters*, *89*(4), 1314-1322.

Chen, W. W., & Song, B. (2010). *Split Hopkinson (Kolsky) bar: design, testing and applications*. Springer Science & Business Media.

Doan, M.L., & Gary, G. (2009). Rock pulverization at high strain rate near the San Andreas fault. *Nature Geoscience, 2*(10), 709.

Dor, O., Ben-Zion, Y., Rockwell, T. K., & Brune, J. (2006a). Pulverized rocks in the Mojave section of the San Andreas Fault Zone. *Earth and Planetary Science Letters*, *245*(3-4), 642-654.

Dor, O., Rockwell, T. K., & Ben-Zion, Y. (2006b). Geological observations of damage asymmetry in the structure of the San Jacinto, San Andreas and Punchbowl faults in Southern California: a possible indicator for preferred rupture propagation direction. *Pure and Applied Geophysics*, *163*(2-3), 301-349.

Griffith, W.A., St. Julien, R.C., Ghaffari, H.O., & Barver, T.J. (2018). A tensile origin for fault rock pulverization. *Journal of Geophysical Research: Solid Earth, 123*(8), 7055-7073.

Huang, J., Xu, S., & Hu, S. (2014). Influence of particle breakage on the dynamic compression responses of brittle granular material. *Mechanics of materials, 68,* 15-28.

Johri, M., Dunham, E. M., Zoback, M. D., & Fang, Z. (2014). Predicting fault damage zones by modeling dynamic rupture propagation and comparison with field observations. *Journal of Geophysical Research: Solid Earth*, *119*(2), 1251-1272.

Kjaernsli B, Sande A. Compressibility of some coarse-grained materials. Proceedings of Wiesbaden European Conference on Soil Mechanics and Foundation Engineering 1963; 1:245-51.

Kolsky, H. (1949). An investigation of the mechanical properties of materials at very high rates of loading. *Proceedings of the physical society. Section B*, *62*(11), 676.

Lamé, G. (1852). 'Leçons sur la Théorie Mathématique de l. *Élasticité des Corps Solides,''Gautheir-Villars, Paris*, 356 p.

Reches, Z. E., & Dewers, T. A. (2005). Gouge formation by dynamic pulverization during earthquake rupture. *Earth and Planetary Science Letters*, *235*(1-2), 361-374.

Rempe, M., Mitchell, T., Renner, J., Nippress, S., Ben-Zion, Y., & Rockwell, T. (2013). Damage and seismic velocity structure of pulverized rocks near the San Andreas Fault. *Journal of Geophysical Research: Solid Earth, 118*(6), 2813-2831.

Rockwell, T., Sisk, M., Girty, G., Dor, O., Wechsler, N., & Ben-Zion, Y. (2009). Chemical and physical characteristics of pulverized Tejon Lookout Granite adjacent to the San Andreas and Garlock faults: implications for earthquake physics. *Pure and Applied Geophysics*, *166*(10- 11), 1725-1746.

Rowe, C. D., & Griffith, W. A. (2015). Do faults preserve a record of seismic slip: A second opinion. *Journal of Structural Geology*, *78*, 1-26.

Sharp, R.V. (1967). San Jacinto fault zone in the Peninsular Ranges of southern California. *Geological Society of America Bulletin, 78*(6), 705-730.

Timoshenko, S. P., & Goodier, J. (1970). Theory of elasticity, 3rd ed, McGraw Hill, 567 p.

Whearty, J. J., Rockwell, T. K., & Girty, G. H. (2017). Incipient pulverization at shallow burial depths along the San Jacinto Fault, Southern California. *Fault Zone Dynamic Processes: Evolution of Fault Properties During Seismic Rupture*, *227*, 1.

Whitman RV. The response of soils to dynamic loading. Report No. 26, Final Report. Vicksburg, Mississippi: U.S. Army Engineer Waterways Experiment Station; 1970.

Wilson, B., Dewers, T., Reches, Z. E., & Brune J. (2005). Particle size and energetics of gouge from earthquake rupture zones. *Nature*, *434*(7034), 749-752.

Xia, K., & Yao, W. (2015). Dynamic rock tests using split Hopkinson (Kolsky) bar system–A review. *Journal of Rock Mechanics and Geotechnical Engineering*, *7*(1), 27-59.

Xu, S., & Ben-Zion, Y. (2017). Theoretical constraints on dynamic pulverization of fault zone rocks. *Geophysical Journal International*, *209*(1), 282-296.